Strong-signal laser operation. II. Specific cases*

J. B. Hambenne and M. Sargent III†
Optical Sciences Center, University of Arizona, Tucson, Arizona 85721
(Received 25 June 1975)

The multimode strong-signal theory of the preceding paper is applied to a number of two- and three-mode cases. A two-mode stability analysis yields strong-signal counterparts to the third-order coupling parameter. Two-mode homogeneous-broadened operation leads to the discussion of population inversion gratings and associated Bragg scattering. Symmetry properties of the equations for the bidirectional ring are examined. Results for Doppler-broadened two-mode special cases and the three-mode locked unidirectional-ring operation are presented. The strong-signal results are compared to those of the third-order and rate-equation–approximation theories. For the bidirectional ring the historical third-order domain of relative excitation from 1.0 to 1.2 is divided into a valid third-order region and a less accurate region. The condition of bistable operation vs monostable operation is seen to be dependent on the relative excitation and the amount of homogeneous broadening. Two types of bistable operation are seen to exist, one where one mode is completely suppressed and another where both modes may have nonzero intensities.

I. INTRODUCTION

In the preceding paper, paper I,[1] we give a Lamb semiclassical theory for multimode, mode-locked laser operation for arbitrarily large intensities. The mode locking condition, i.e., equality of frequency spacings between adjacent modes, causes population pulsations generated in the nonlinear atomic response to be integer multiples of the adjacent mode spacings. This allows the atomic response to be written in terms of a Fourier series, which reduces coupled differential equations of motion to algebraic equations which are expressible in terms of a continued fraction. Numerical analysis of the equations is discussed. A unidirectional ring configuration is assumed for the general multimode case so that the more complicated spatial dependence of standing waves is avoided.

The present paper considers several simple examples of the general multimode case. Numerical results are presented and physical interpretations of equations are motivated.

As discussed in paper I, the unidirectional ring, two-mode results contain the single-mode standing-wave and the bidirectional ring configurations as special cases when appropriate transformations are made. We have devoted a substantial portion of the present work to discussion of the nature and interrelationship of these cases. The bidirectional ring laser has been of particular interest. Historically this was motivated by a desire to duplicate the classic experiment of Sagnac (1911) to detect absolute rotation.[2] Inspired by the extremely-well-defined frequency and stability of the laser, the experiment was duplicated with the laser media in one arm of the classical light path.[3] Theoretical considerations aside, the practical significance of applications of this fledgling rate gyro were immediately apparent; however, enthusiasm was quickly dampened when two phenomena that were experimentally observed seemed to drastically limit the bidirectional ring laser's use as a rate gyro. These were mode locking and mode inhibition (single-traveling-wave operation). In both cases the beat note vanishes, thus precluding use as a rate gyro. These two effects were resolved with the application of semiclassical perturbation theory to the bidirectional ring laser problem.[4] The mode-locked operation experimentally observed was explained by the assumption of backscattering of one traveling wave into the other by laser mirrors, particles in the laser media, etc. Theories were developed which contained provisions for this form of backscattering.[5] More recently,[6] bistable unidirectional operation was explained in terms of backscattering by induced population-inversion gratings, an effect shown to be included in the third-order theory. This effect is also important in various types of saturation spectroscopy.

In Sec. II, a summary of the pertinent equations from the preceding paper[1] is given. In Sec. III, two-mode strong-signal stability and competition analysis is presented. We summarize third-order theory and discuss the deviation of a mode's intensity from the average mode intensities in terms of a concept called fractional intensity splitting. A small-vibration analysis for strong signals yields two strong-signal counterparts to the coupling parameter. In Sec. IV, two-mode homogeneous-broadened operation leads to the discussion of population-inversion gratings and associated Bragg scattering. This may result in bistable unidirectional operation. The transition to the Doppler-limited case is introduced. In

Sec. V, two-mode Doppler-broadened results are presented and compared to the rate-equation approximation (REA) and third-order results. A discussion of the observed differences is motivated by an examination of several important symmetry properties of the equations describing the bidirectional ring laser. For that laser, the historical third-order domain of relative excitation from 1.0 to 1.2 is divided into a valid third-order region and a less accurate region referred to as the pseudo-third-order domain. The condition of bistable operation versus monostable operation is seen to be dependent on the relative excitation and the amount of homogeneous broadening. Two types of bistable operation are seen to exist, one discussed in the past,[6] where one mode is completely suppressed, and another, new here, where both modes may have nonzero intensities. In Sec. VI, three-mode locked operation is presented, and the results are compared with those of Salomaa and Salomaa,[7] who were not able to obtain strong-signal mode-locked solutions. In addition, solutions for other laser parameters are discussed. An approximation is made similar to a rate equation approximation in which the population pulsation (dc bias) contribution to the dc (average) population inversion is kept. This indicates the relative importance of the bias terms versus the other modulator parameters.

II. ELECTROMAGNETIC FIELD EQUATIONS AND POLARIZATION OF THE MEDIUM

In this section we summarize pertinent equations from the preceding paper, so as to define notation and give a self-contained presentation for the reader not interested in the derivation.

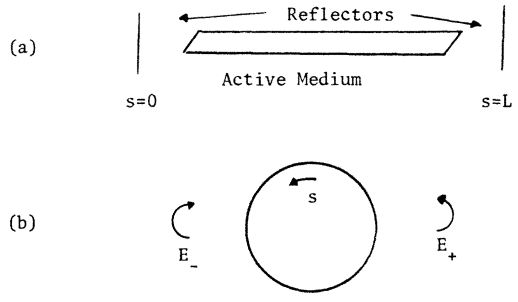

FIG. 1. (a) Diagram of two-mirror standing-wave laser showing reflectors in plane perpendicular to the laser (s) axis and active medium between the reflectors. Brewster windows are sketched on the ends of the active medium to help enforce the condition that only one polarization component of the electric field exists, as assumed in this paper. (b) Corresponding ring laser configuration. The optical path may consist of a single-turn or multiturn optical fiber as well as the usual polygon. The active medium may be integral to the fiber or more localized as in (a).

We have from Ref. 1 [Eqs. (5) and (6) of paper I, hereafter denoted (I 5), (I 6), etc.] the self-consistency equations for the field[8]

$$\dot{E}_n = -\tfrac{1}{2}(\nu/Q_n)E_n - \tfrac{1}{2}(\nu/\epsilon_0)\,\mathrm{Im}\mathcal{P}_n\,, \tag{1a}$$

$$\nu_n + \dot{\phi}_n = \Omega_n - \tfrac{1}{2}(\nu/\epsilon_0)(1/E_n)\,\mathrm{Re}\mathcal{P}_n\,, \tag{1b}$$

where the electric field mode amplitudes are determined from the electric field $E(s,t)$ by

$$E(s,t) = \tfrac{1}{2}\sum_{n=1}^{N} E_n e^{-i(\nu_n t + \phi_n)} U_n(s) + \text{c.c.}, \tag{2}$$

and the complex polarization coefficient $\mathcal{P}_n$ is defined by

$$P(s,t) = \tfrac{1}{2}\sum_{n=1}^{N} \mathcal{P}_n(t) e^{-i(\nu_n t + \phi_n)} U_n(s) + \text{c.c.}, \tag{3}$$

where $P(s,t)$ is the polarization of the medium and N is the number of modes.

The mode functions $U_n(s)$ are determined by the laser configuration (see Fig. 1) and type of operation. For the ring laser

$$U_n(s) = e^{iK_n s}, \quad K_n = 2n\pi/L, \tag{4}$$

where L is the round trip cavity length and n is the mode number which can be either + or − for the bidirectional ring, but only + for the unidirectional ring. For the standing-wave laser

$$U_n(s) = \sin K_n s, \quad K_n = n\pi/L. \tag{5}$$

For the bidirectional ring it has been shown by Menegozzi and Lamb,[9] for example, that the effects of small rotation rates on the self-consistency equations is to introduce a shift in the empty-cavity resonance frequencies $\Omega_n = |Kn|c$ by an amount $2A\dot{\theta}\Omega_n/Lc$, where A is the area enclosed by the laser path and $\dot{\theta}$ is the laser rotation rate. Traveling-wave modes are up (ν_-) or down (ν_+) shifted depending on whether they are going in the opposite or same direction as the cavity rotation. Hence in the self-consistency equations

$$\Omega_n \to \Omega_n - (2TA\dot{\theta}\Omega_n/Lc)\,\mathrm{sgn}K_n = \Omega_n - \tfrac{1}{2}\Delta_r\,\mathrm{sgn}K_n\,, \tag{6}$$

where T is the number of turns if a multiturn loop is used.

We assume the medium consists of independent two-level atoms. Spontaneous lifetimes γ_a and γ_b describe decay for the upper and lower levels, respectively. The decay of the dipole moment term is described by the constant γ. We describe the medium by a population matrix $\rho(s, K\nu, t)$ and, as in paper I, Fourier-analyze the population difference D and polarization element ρ_{ab} in terms

of the fundamental population-pulsation frequency Δ and its harmonics. This yields algebraic equations relating the population-pulsation Fourier coefficients d_k and the polarization Fourier components p_m. These equations give a recursion relation for the d_k and lead to a continued-fraction solution for the population-difference Fourier coefficients in terms of the ratios r_l,

$$r_l \equiv d_l / d_{l-1}. \tag{7}$$

For two-mode operation we have the recursion relation

$$c_{1,k} d_{k+1} + c_{0,k} d_k + c_{-1,k} d_{k-1} = 0, \tag{8}$$

with the coefficients defined by

$$c_{-1,k} = \gamma_{ab} (I_1 I_2)^{1/2} [\mathfrak{D}(\nu_{1+k} - \omega) + \mathfrak{D}(\omega - \nu_{2-k})], \tag{9a}$$

$$c_{1,k} = \gamma_{ab} (I_1 I_2)^{1/2} [\mathfrak{D}(\nu_{2+k} - \omega) + \mathfrak{D}(\omega - \nu_{1-k})], \tag{9b}$$

$$c_{0,k\neq 0} = \left(1 - \frac{\delta_{k,0}}{d_0}\right)[\mathfrak{F}(k\Delta)]^{-1} + \gamma_{ab} \sum_{n=1}^{2} I_n [\mathfrak{D}(\nu_{n+k} - \omega) + \mathfrak{D}(\omega - \nu_{n-k})]. \tag{9c}$$

The population coefficients $d_1 = d_{-1}^* = d_0 r_1$, and

$$\mathfrak{F}(k\Delta) = \tfrac{1}{2}[\mathfrak{D}_a(2kKv) + \mathfrak{D}_b(2kKv)] \gamma_a \gamma_b / \gamma_{ab}, \tag{10}$$

where

$$\mathfrak{D}_x(\Delta\omega) = (\gamma_x + i\Delta\omega)^{-1} \tag{11}$$

and

$$\nu_{1-k} = \nu_1 - k\Delta, \tag{12}$$

where Δ is the fundamental population-pulsation frequency and where the dimensionless intensity is given by

$$I_n = \tfrac{1}{2}(\wp \mathcal{E}/\hbar)^2 (1/\gamma_a \gamma_b), \tag{13}$$

where $\wp$ is the electric dipole matrix element between the upper and lower levels.

From the recursion relation for the d_k, the dc population-difference coefficient d_0 is given by

$$d_0 = 1/(1 + S_h + S_p), \tag{14}$$

where S_h is the saturation due to hole burning, given by

$$S_h = 2(\gamma_{ab}/\gamma)[I_1 \mathfrak{L}(\omega - \nu_1) + I_2 \mathfrak{L}(\omega - \nu_2)], \tag{15}$$

where

$$\mathfrak{L}(\Delta\nu) = \gamma^2 / [\gamma^2 + (\Delta\omega)^2],$$

and S_p is the saturation due to population pulsations, given by

$$S_p = c_{1,0} r_1 + \text{c.c.} \tag{16}$$

The ratios r are calculated in terms of the continued fraction

$$r_l = \frac{-c_{-1,l}}{c_{0,l} + c_{1,l} r_{l+1}} = \frac{-c_{-1,l}}{c_{0,1} - c_{1,1} c_{-1,2} / (c_{0,2} + c_{1,2} r_3)}, \tag{17}$$

etc.

Similarly, the general polarization coefficient [(50) of I] is given by

$$\mathcal{P}_n = -\epsilon_0 \mathfrak{N} [Q\sqrt{\pi} Z_i(\gamma)]^{-1} \times \sum_m E_m \exp[i(\phi_n - \phi_m)] \times \int_{-\infty}^{\infty} d\omega \exp\left(\frac{-(\omega - \omega_0)^2}{(\Delta\omega)^2}\right) \mathfrak{D}(\omega - \nu_n) d_{m-n}. \tag{18}$$

The polarization coefficients $\mathcal{P}_n$ for two modes are given by

$$\mathcal{P}_1 = -i\epsilon_0 \frac{\mathfrak{N}}{Q\sqrt{\pi} Z_i(\gamma)} \int_{-\infty}^{\infty} d\omega \exp\left(\frac{-(\omega - \omega_0)^2}{(\Delta\omega)^2}\right) \times \mathfrak{D}(\omega - \nu_1)(E_1 d_0 + E_2 d_1), \tag{19a}$$

$$\mathcal{P}_2 = -i\epsilon_0 \frac{\mathfrak{N}}{Q\sqrt{\pi} Z_i(\gamma)} \int_{-\infty}^{\infty} d\omega \exp\left(\frac{-(\omega - \omega_0)^2}{(\Delta\omega)^2}\right) \times \mathfrak{D}(\omega - \nu_2)(E_2 d_0 + E_1 d_{-1}), \tag{19b}$$

where $\omega = kv$, and where it may be noted that keeping only the first term in the continued fraction corresponds to the REA as $r_1 = 0$; hence d_1 and $S_p = 0$.

Appropriate transformations of the fundamental population-pulsation frequency (Δ) and the Doppler-shifted mode frequencies allow these two-mode equations to be used for the two-mirror single-mode standing-wave laser and the bidirectional ring laser. These transformations are summarized in Table I. For the standing-wave

TABLE I. Summary of the parameters Δ and ν for the two-mode cases.

	Unidirectional	Standing wave	Bidirectional
Δ	$\nu_2 - \nu_1$	$2kv$	$\nu_- - \nu_+ + 2kv$
ν_1	$\nu_1 - kv$	$\nu - kv$	$\nu_+ - kv$
ν_2	$\nu_2 - kv$	$\nu + kv$	$\nu_- + kv$

laser we have the additional requirements

$$E = E_1 + E_2, \quad (I_1 = I_2 = \tfrac{1}{4}I),$$

$$\mathcal{P} = \mathcal{P}_1 + \mathcal{P}_2,$$

$$\theta_1 \to \theta_1 + \tfrac{1}{2}\pi, \quad \theta_2 \to \theta_2 - \tfrac{1}{2}\pi.$$

III. TWO-MODE STABILITY AND COMPETITION ANALYSIS

In this section we summarize two-mode operation as given by third-order perturbation theory. This treatment provides simple analytic descriptions of various phenomena and hence provides useful points of reference for our strong-signal discussions. We also introduce here the notion of the fractional intensity splitting, that is, the ratio of the difference in the mode's intensities to their average value. This concept is particularly useful in describing the strong competition that occurs, for example, in the bidirectional ring laser operating at low relative excitation near symmetric tuning. This section closes with a generalization of two-mode stability analysis to strong-signal operation. Two extensions of the third-order coupling parameter are introduced, one determining stability and the other giving a measure of cross saturation to self-saturation.

A. Two-mode operation in third-order theory

In the third-order limit, both characteristics are described by the single parameter C. The third-order intensity equations of motion are (for the unidirectional and bidirectional ring cases) [from Ref. 10, Eqs. (11–13) and (11–14)]

$$\dot{I}_1 = 2I_1(\alpha_1 - \beta_1 I_1 - \theta_{12} I_2), \tag{20a}$$

$$\dot{I}_2 = 2I_2(\alpha_2 - \beta_2 I_2 - \theta_{21} I_1), \tag{20b}$$

where the coefficients are defined in Table 11-1 of Ref. 10 for Doppler-broadened media and in general by O'Bryan and Sargent.[11] The α_n are the linear net gains of the modes (gain minus loss), the β_n are the self-saturation coefficients, and the θ_{nm} are cross-saturation coefficients. The stationary-state solutions ($\dot{I}_n = \dot{I}_m = 0$) are characterized by the coupling parameter (C) given by

$$C = \theta_{12}\theta_{21}/\beta_1\beta_2. \tag{21}$$

For weak coupling ($C < 1$), these equations yield the solutions given by

$$I_1 = \left(\frac{\alpha_1}{\beta_1} - \frac{\theta_{12}}{\beta_1}\frac{\alpha_2}{\beta_2}\right)\frac{1}{1-C}, \tag{22a}$$

$$I_2 = \left(\frac{\alpha_2}{\beta_2} - \frac{\theta_{21}}{\beta_2}\frac{\alpha_1}{\beta_1}\right)\frac{1}{1-C}. \tag{22b}$$

Let us consider in particular the case for which the saturation terms are approximately equal, i.e., $\beta_1 = \beta_2 = \beta$ and $\theta_{12} = \theta_{21} = \theta$, and for which a fractional gain difference between the modes exists, i.e., $\alpha_1 = \alpha$ and $\alpha_2 = \alpha + \epsilon$. This occurs, for example, near symmetric tuning in the Doppler limit for the bidirectional ring laser. With these assumptions the mode intensities of (22) become

$$I_1 = \alpha\left(\frac{1}{\beta+\theta} - \frac{\epsilon}{\alpha}\frac{\theta}{\beta^2}\frac{1}{1-C}\right),$$

$$I_2 = \alpha\left(\frac{1}{\beta+\theta} + \frac{\epsilon}{\alpha}\frac{\theta}{\beta^2}\frac{1}{1-C}\right).$$

These yield an average steady-state intensity $\alpha/(\beta+\theta)$, which in the case of equal self-saturation and cross saturation is just one-half the intensity α/β predicted for a mode oscillating by itself. Thus for equal gain we obtain equal intensities (excluding any hysteresis effects and associated bistable operation). The fractional intensity splitting is given by

$$\frac{I_2 - I_1}{\frac{1}{2}(I_2 + I_1)} = 2\frac{\epsilon}{\alpha}\frac{\beta+\theta}{(1-C)} = 2\frac{\epsilon}{\alpha}\frac{\theta}{(\beta-\theta)}, \tag{23}$$

that is, it is proportional to the fractional gain difference ϵ/α and inversely proportional to the quantity $1 - C$.

B. Mode stability and the coupling parameter in the strong-signal laser theory

In the third-order theory the equations of motion for the mode intensities contain terms that lend themselves readily to simple physical interpretation, namely, the linear net gain of an individual mode α_n, self-saturation β_n (the saturation of a mode intensity on its own gain), and cross saturation θ_{nm} (the saturation of one mode m on the gain of mode n). These third-order parameters are a three-fold degenerate case of the corresponding strong-signal parameters. Specifically, we can define three classes of parameters: (i) near threshold (where third-order theory is valid), (ii) linearized small signal parameters taken about a (generally) strong-signal operating point, and (iii) large signal parameters at such a point.

The general problem of multimode operation deals with the question of which modes may actually oscillate in the laser, i.e., represent stable solutions to the intensity equations of motion. To resolve this question, a small-vibration analysis is usually performed. The influence of one mode on another is expressed in terms of a coupling parameter C which, for the two-mode case, is the ratio of the product of the cross-saturation terms to the product of the self-saturation terms. The third-order intensity equations of motion and

the coupling parameter are given by (20) and (21). In the case of the third-order theory the equations represent an expansion about threshold intensity, and, consequently, are not valid for strong-signal results. For the case of stability parameters a similar formalism may be developed for strong-signal theories by expanding about the steady-state intensities. We now do this for two-mode operation.

The amplitude self-consistency equation [(I5)] may be written in terms of the susceptibility χ_n, where

$$\mathcal{P}_n(t) = \epsilon_0 \chi_n E_n(t) = \epsilon_0(\chi_n' + i\chi_n'')E_n(t), \tag{24}$$

as

$$\dot{E}_n(t) = -\tfrac{1}{2}(\nu/Q_n)E_n(t) - \tfrac{1}{2}\nu_n \chi_n'' E_n(t).$$

From this equation for mode amplitudes we obtain an equation of motion for the mode intensities,

$$\dot{I}_n = -\nu_n I_n \chi_n'' - (\nu_n/Q_n)I_n, \tag{25}$$

where for steady-state intensities we have the identity

$$\dot{I}_n^S \equiv 0 = -\nu_n I_n^S \chi_n''^S - (\nu/Q_n)I_n^S. \tag{26}$$

Let us now consider a small-vibration analysis about the steady-state mode intensities, i.e., let the mode intensities be perturbed by ϵ_n. Inserting these values of intensities into the equations of motion, we have

$$\begin{aligned}\dot{I}_n &\equiv I_n^S + \dot{\epsilon}_n \\ &= (I_n^S + \epsilon_n)\chi_n''^S(I_n^S + \epsilon_n, I_m^S + \epsilon_m) - (\nu/Q_n)(I_n^S + \epsilon_n).\end{aligned}$$

Expanding χ_n'' in a first-order Taylor series about its steady-state value, we obtain

$$\chi_n''(I_n, I_m) = \chi_n''^S + \epsilon_n \frac{\partial \chi_n''^S}{\partial I_n} + \epsilon_m \frac{\partial \chi_n''^S}{\partial I_m}.$$

This expression for χ_n'' and the perturbed equations of motion yield the following expression for the perturbed mode intensities:

$$\dot{I}_n = \dot{\epsilon}_n = -\nu_n(I_n^S + \epsilon)\left(\chi_n''^S + \epsilon_n \frac{\partial \chi_n''^S}{\partial I_n} + \epsilon_m \frac{\partial \chi_n''^S}{\partial I_m} + \frac{1}{Q_n}\right).$$

For nonzero I_n^S, keeping the first-order terms in ϵ and using the identity in (26), we have the linearized equation of motion for the small signal perturbation,

$$\dot{\epsilon}_n = -\nu_n I_n^S\left(\epsilon_n \frac{\partial \chi_n''^S}{\partial I_n} + \epsilon_m \frac{\partial \chi_n''^S}{\partial I_m}\right). \tag{27}$$

If I_n^S is zero, we have

$$\dot{\epsilon}_n = -\nu_n \epsilon_n[\chi_n''^S(0, I_m) + 1/Q_n]. \tag{28}$$

We may generalize the third-order terms and obtain the stability coefficients corresponding to the (small signal) self-saturation β_n and cross-saturation θ_{nm} at the strong-signal point (I_n^S, I_m^S),

$$\begin{aligned}\beta_n \leftarrow \beta_n^{Sm} &\equiv \frac{\nu_n}{2}\frac{\partial \chi_n''^S}{\partial I_n}\bigg|_{I_n^S, I_m^S}, \\ \theta_{nm} \leftarrow \theta_{nm}^{Sm} &\equiv \frac{\nu_n}{2}\frac{\partial \chi_n''^S}{\partial I_m}\bigg|_{I_n^S, I_m^S}.\end{aligned} \tag{29}$$

Equation (27) may be written as

$$\dot{\epsilon}_n = -2I_n(\beta_n^{Sm}\epsilon_n + \theta_{nm}^{Sm}\epsilon_m).$$

These equations form a set of coupled first-order differential equations for the small signal perturbation ϵ_n. These will have solutions with exponentially decaying envelopes if the roots of the characteristic equation have real negative parts. We find two conditions,[7]

$$I_1\beta_1^{Sm} + I_2\beta_2^{Sm} > 0, \quad \frac{1 - C^{Sm}}{I_1 I_2 \beta_1^{Sm}\beta_2^{Sm}} > 0, \tag{30}$$

where the stability coupling parameter

$$C^{Sm} \equiv \frac{\theta_{nm}^{Sm}\theta_{mn}^{Sm}}{\beta_n^{Sm}\beta_m^{Sm}} = \left[\frac{\partial \chi_n''^S}{\partial I_m}\frac{\partial \chi_m''^S}{\partial I_n}\Big/\frac{\partial \chi_n''^S}{\partial I_n}\frac{\partial \chi_m''^S}{\partial I_m}\right]_{I_n^S, I_m^S}. \tag{31}$$

Usually the first condition is fulfilled and $I_1 I_2 \beta_1^{Sm}\beta_2^{Sm} > 0$, so we are left with the "weak-coupling" condition

$$C^{Sm} < 1,$$

which corresponds to that used in the past.[10]

For the third-order regime, the stability coefficients are the β's and θ's. They give as well the degree of self-saturation and cross saturation. For larger intensities we use the $\partial\chi_n''/\partial I_m$ for stability purposes, but these partial derivatives do not give accurate indications of self-saturation or cross saturation except near threshold. To get an idea of the strong-signal self-saturation and cross saturation, we consider the susceptibilities $\chi_n''(I_1, I_2)$ directly in the remainder of this section.

For the case of zero intensities we have the threshold net gain coefficient

$$\alpha_n = -\tfrac{1}{2}\nu[\chi_n''(0,0) + 1/Q_n] \tag{32}$$

which is the same for third-order and the strong-signal theories. If one mode is zero, then for the other we have the threshold cross-saturated linear net gain

$$\alpha_n' = -\tfrac{1}{2}\nu[\chi_n''(0, I_m) + 1/Q_n], \tag{33}$$

which is the threshold gain mode n sees in the presence of the (in general) strong-signal mode intensity I_m. This reduces to the third-order effective linear net gain in the limit of small I_m,

$$\alpha_n' = \alpha_n - \theta_{nm} I_m. \tag{34}$$

We can find even for the case of a strong-signal operating point a large signal parameter θ_{nm}^{LD} by using (34) as a definition with (32) and (33),

$$\theta_{nm}^{LD} = -\tfrac{1}{2}\nu[\chi_n''(0,0) - \chi_n''(0,I_m)]/I_m. \tag{35}$$

Similarly we can define a large signal self-saturation coefficient

$$\beta_n^{LD} = -\tfrac{1}{2}\nu[\chi_n''(0,0) - \chi_n''(I_n,0)]/I_n \tag{36}$$

The strong-signal result for the (large signal degenerate) third-order equation for the saturated net gain is

$$\alpha_1 - \beta_1^L I_1 - \theta_{12}^L I_2$$

where the large signal parameter β_1^L is a function of I_2, not just of I_1, and θ_{12}^L is a function of I_1, not just of I_2. We may define a decoupled approximation when

$$\beta_1^L \cong \beta_1^{LD} \neq f(I_2), \quad \theta_{12}^L \cong \theta_{12}^{LD} \neq f(I_1).$$

In this approximation the saturated net gain is

$$\alpha_1 - \beta_1^{LD} I_1 - \theta_{12}^{LD} I_2. \tag{37}$$

We may define an alternate strong signal C^{LD} that expresses the ratio of the above decoupled strong-signal saturation coefficients,

$$C^{LD} = \theta_{12}^{LD}\theta_{21}^{LD}/\beta_1^{LD}\beta_2^{LD}. \tag{38}$$

This may be illustrated for the case of a homogeneously-broadened, equal-tuned bidirectional ring laser ($\nu_+ = \nu_- = \nu$). We have for the susceptibility (from the Appendix)

$$\chi_i'' \propto \frac{1}{4\mathfrak{L}(\omega-\nu)} I_i \left(1 - \frac{1 + 2\mathfrak{L}(\omega-\nu)(I_j - I_i)^2}{1 + 2S_h + 4\mathfrak{L}^2(\omega-\nu)(I_j - I_i)^2}\right), \tag{39}$$

where $S_h = 2\mathfrak{L}(\omega-\nu)(I_i + I_j)$. This yields the competition parameter

$$C^{LD} = \frac{4[1+(\omega-\nu)I_i][1+(\omega-\nu)I_j]}{[1+2(\omega-\nu)I_i][1+2(\omega-\nu)I_j]}. \tag{40}$$

In the limit of small intensities this ratio equals 4, which agrees with the third-order result. In the limit of large intensities $C^{LD} = 1$, showing a decrease with increasing intensities. However, at large intensities, the decoupled approximation (37) is no longer valid. When not in the valid third-order region the parameters C^{Sm} (31) or C^{LD} (38) may exhibit anomalous behavior. For example, C^{Sm} may assume positive or negative values, or approach 0 or $\pm\infty$, as may also β^{Sm} and θ^{Sm} of (29).

The third-order theory gives analytical results for the stability parameters. Since the strong-signal results are obtained by numerical means, these parameters must also be evaluated numerically. The Newton-Raphson iterative procedure (see Sec. VII of I) for solving the intensity-determining equations requires the calculation of such partial derivatives. During a frequency scan of the laser cavity, if the frequency step is small enough such that the mode intensities do not change appreciably from one point to the next, the values of the partial derivatives may be used to calculate the coupling parameter. This saves the coupling time that would be required to evaluate the partial derivatives at the final stationary-state values of intensity.

IV. TWO-MODE OPERATION IN THE PRESENCE OF LITTLE OR NO DOPPLER BROADENING

In this chapter we consider two-mode bidirectional and unidirectional, homogeneously-broadened ring laser operation and then discuss the transition to the Doppler-broadened case. For the homogeneous case, both running waves interact with the same atoms yielding self-saturation equal to the cross saturation caused by population depletion. In the absence of other kinds of cross saturation this equality produces neutral coupling. Hence the additional cross saturation introduced by coherence terms, e.g., population pulsations, plays a critical role in determining whether the coupling is strong or weak.

For the equal-tuned ($\nu_+ = \nu_- = \nu$) bidirectional ring and standing-wave, two-mirror lasers, the two oppositely directed running waves comprising the electric field add in the medium, yielding a standing wave, and burn spatial holes in the population inversion as illustrated in Fig. 2. This corrugated inversion pattern acts like a Bragg grating to reflect one running wave back into the

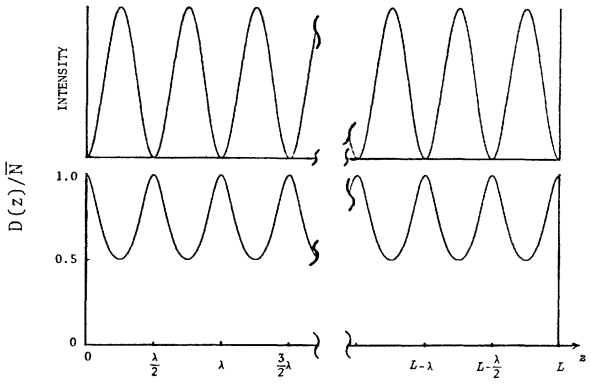

FIG. 2. Graph of normalized population difference vs laser axial coordinate. Note that the grating formed by the spatial holes is out of phase with the intensity.

other. For stationary atoms this grating is precisely out of phase with the standing-wave pattern, and the net reflected wave subtracts from the similarly directed running wave. Thus in addition to the usual population-depletion part the cross saturation contains a Bragg-scattering term. In the equal-tuning case, the two saturation terms are identical and add, giving a total cross saturation twice as big as the self-saturation. Hence strong coupling occurs. The coupling parameter in third order is depicted in Fig. 3, with a value of 4 for $Ku = 0$ and any average detuning. The result is bistable, single-traveling-wave (STW) operation. Either mode may suppress the other, and which one wins depends on the linear gains and the initial intensities. For nonzero rotation rate ($\nu_+ - \omega = \omega - \nu_- \neq 0$), the electric field remains a standing wave in the nonrotating, i.e., not laser, frame. Hence the induced grating moves with respect to the medium and Doppler shifts the scattered waves from ν_+ to ν_- (or vice versa) in a fashion analogous to Brillouin scattering.

The unidirectional ring does not have a slowly moving grating, but rather has population pulsations at the intermode frequency. In the third-order theory these pulsations increase or decrease the cross saturation according to the sign of the expression

$$\frac{1}{\gamma_a}\mathfrak{L}_a(\Delta_r)\left(1-\frac{\Delta_r^2}{2\gamma\gamma_a}\right)+\frac{1}{\gamma_b}\mathfrak{L}_b(\Delta_r)\left(1-\frac{\Delta_r^2}{2\gamma\gamma_b}\right) \qquad (41)$$

which follows from the coefficients in Table VII of Ref. 11 (for symmetric tuning). A negative sign gives weak coupling and two modes may oscillate. A positive sign gives strong coupling and only one mode oscillates.

As the medium is Doppler broadened, for symmetric tuning (i.e., zero average detuning), each velocity ensemble sees a different grating. Figure 4 (from Ref. 12) illustrates the spatial gratings for various velocity ensembles. The curve for $Kv = 0$ is just that for the homogeneous case. The series of curves illustrate two effects that change the Bragg-scattering contribution to the cross saturation. Apart from the Maxwellian distribution factor, the amplitude of the individual gratings decreases as a function of $Kv + \frac{1}{2}\Delta_r$ for it is the ensemble with $v = -\Delta_r/2K$ that is stationary with respect to the standing-wave pattern. Other ensembles move through the standing-wave field and the amplitude of their population-difference gratings is restricted by the bandwidth of the medium, i.e., γ_a and γ_b. This is a more detailed statement than "the atoms tend to see an average field." Secondly, the gratings are shifted with respect to the $v = -\Delta_r/2K$ grating, thereby yielding variously phased scattered waves that tend to destructively interfere. The combination of this destructive interference and the reduction in grating amplitudes produces an overall smaller Bragg contribution to the cross saturation for large Doppler widths. Hence the coupling parameter C decreases for increasing Ku, although for some large, finite values of Ku the reflected wave may add slightly, allowing the coupling parameter to be barely less than unity. In the extreme Doppler limit the Bragg contribu-

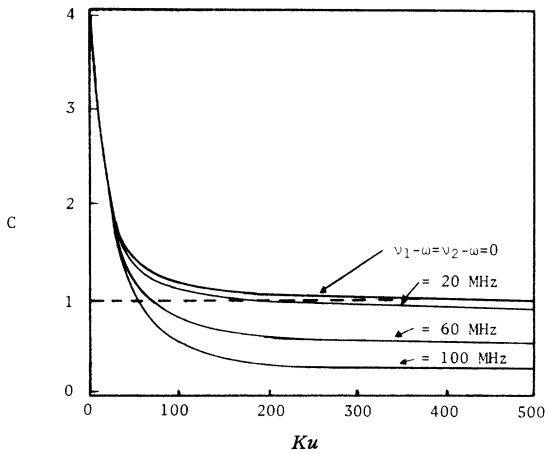

FIG. 3. Coupling parameter C of Eq. (21) plotted vs Doppler-width parameter Ku (in MHz) for indicated average detuning. Upper- and lower-level decay rates are 15.5 and 41 MHz respectively, and the dipole decay rate ($1/T_2$) is 100 MHz. The dashed line gives $C=1$, the dividing line between strong ($C > 1$) and weak coupling.

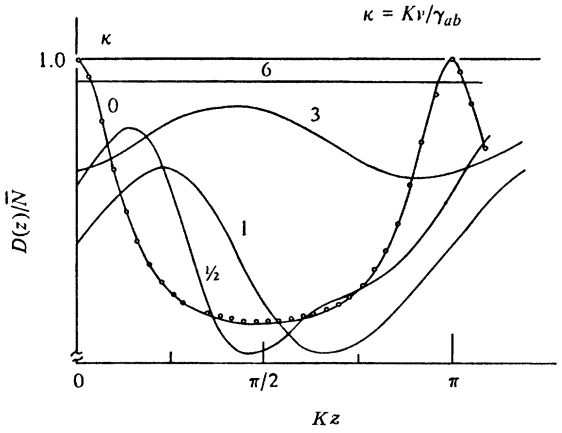

FIG. 4. Graph of normalized population difference vs spatial phase Kz along axis. Spatial holes burned by field intensity for nonmoving atoms are seen to wash out for rapidly moving atoms. ($Ku >> \gamma$ and $\gamma = \gamma_{ab}$, standing-wave laser.) From Stenholm and Lamb (Ref. 12, reproduced with permission).

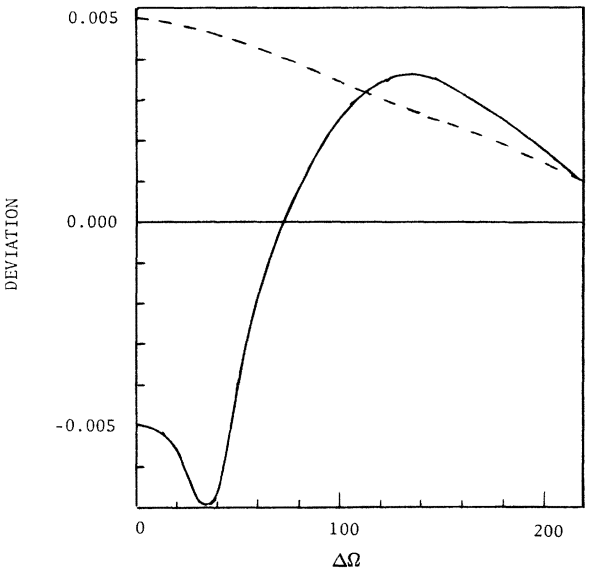

FIG. 5. Graph of the deviation of coupling parameters from the third-order Doppler-limit result vs average cavity detuning for the bidirectional ring laser. The dashed curve is the deviation of the third-order generally broadened coupling parameter. The solid curve is the deviation of the strong-signal parameter C^{Sm}. The laser parameters are $\Delta_r = 15$ MHz, $\gamma_a = 20$ MHz, $\gamma_b = 40$ MHz, $\gamma = 100$ MHz, $Ku = 1010$ MHz, and relative excitation $= 1.05$.

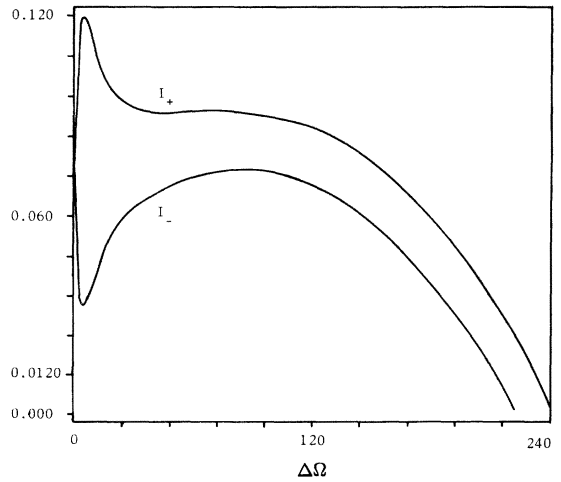

FIG. 6. Graph of the strong-signal theory bidirectional ring laser intensities vs average cavity detuning for a relative excitation of 1.05. Note that complete mode inhibition does not occur in the strong-interaction region about the origin as in third-order theory. Rotational frequency splitting $\Delta_r = 15$ MHz. The laser parameters are $\gamma_a = 20$ MHz, $\gamma_b = 40$ MHz, $\gamma = 100$ MHz, $Ku = 1010$ MHz. For convenience we quote these in MHz when actually they are 2π MHz.

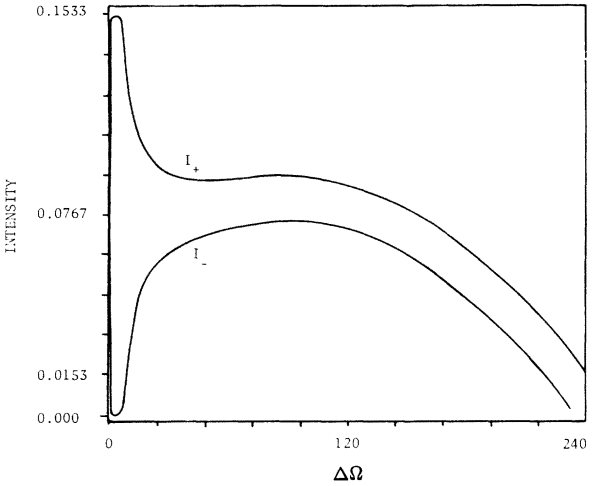

FIG. 7. Graph of the REA theory bidirectional ring laser intensities vs average cavity detuning for a relative excitation of 1.05. Laser parameters are the same as in Fig. 6.

tion is zero and the coupling parameter is unity. The sensitivity of the coupling parameter to the Bragg contribution is seen in Fig. 5, which compares the strong-signal continued fraction C^{Sm} to the third-order Doppler broadened C for a relative excitation of 1.05. Both of these curves deviate from the third-order Doppler-limit result of the square of a simple Lorentzian of average detuning [Eqs. (11–17) of Ref. 10]. The third-order broadened result predicts strong coupling at symmetric tuning while the strong-signal result predicts weak coupling.

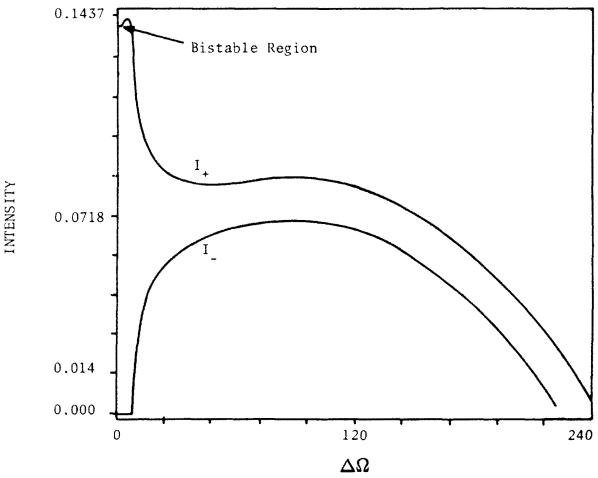

FIG. 8. Graph of the third-order generally broadened theory bidirectional ring laser intensities vs average cavity detuning for a relative excitation of 1.05. Note the bistable region near the origin. The laser parameters are the same as in Fig. 6.

For nonzero average detuning in Doppler-broadened media, the running waves no longer share a common set of atoms, thereby decreasing the population-depletion contribution to the cross saturation and therefore the coupling parameter C as well. This is illustrated in Fig. 3, where for a given value of $Ku \neq 0$ the curves for increasing detuning are seen to yield decreasing values for C.

V. TWO-MODE DOPPLER-BROADENED OPERATION

An example of the results for Doppler-broadened media is given in Figs. 6–9, where the relative excitation is 1.05 and the figures correspond to the strong-signal, REA, and third-order theories, respectively. There is considerable difference between these figures primarily in the fractional intensity splitting near symmetric tuning. For example, the third-order theory predicts bistable operation plus associated mode inhibition at symmetric tuning, but the strong-signal theory predicts equal intensities. An explanation of these differences and useful physical insight into the bidirectional ring laser may be obtained by examining symmetry properties inherent in some of the equations describing the solution to the laser problem. We choose first to illustrate this by the hole-burning terms (S_h) in the population difference of (15),

$$S_h = 2(\gamma_{ab}/\gamma)\left[E_+^2 \mathfrak{L}(\omega - \nu_0 + \tfrac{1}{2}\Delta_r + Kv) + E_-^2 \mathfrak{L}(\omega - \nu_0 - \tfrac{1}{2}\Delta_r - Kv)\right]. \quad (42)$$

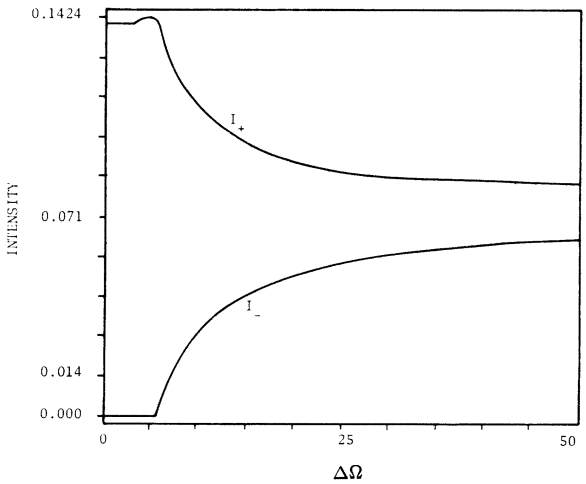

FIG. 9. Graph of the third-order Doppler-limit theory bidirectional ring laser intensities vs average cavity detuning for relative excitation of 1.05. The region near the origin is similar to that in Fig. 8 but is not bistable. Laser parameters are the same as in Fig. 6, except $Ku = \infty$.

The first term is resonant with atoms which have

$$Kv = -(\omega - \nu_0) - \tfrac{1}{2}\Delta_r = (\text{detuning}) - (\text{rotational shift}), \quad (43)$$

and the second for

$$Kv = (\omega - \nu_0) - \tfrac{1}{2}\Delta_r = -(\text{detuning}) - (\text{rotational shift}). \quad (44)$$

For zero average detuning, both terms interact with the same group of atoms, namely, those with Kv approximately equal to one-half the rotational beat frequency ($\frac{1}{2}\Delta_r$). Thus a single traveling hole is burned in the population difference and is shifted from the origin of the velocity distribution by an amount equal to $\frac{1}{2}\Delta_r/K$. This hole is traveling in the laser frame of reference, i.e., the media. However, depending upon the approximations used and the extent that the laser configuration is circular, it may be stationary in an inertial rotational frame of reference. Secondary resonances and resulting holes (such as contribute to the population-pulsation term S_p), in general, travel in either frame of reference. The single rotationally shifted traveling hole for S_h should be compared with the single standing hole burned at the origin for zero detuning in the case of the familiar two-mirror, standing-wave laser.

For the case of nonzero average detuning, (42) and (43) for the bidirectional ring laser reveal that two holes exist symmetrically located with respect to the rotationally shifted zero-average-detuning hole and are shifted from it by an amount equal to the magnitude of the average detuning. Thus these two holes are asymmetrically posi-

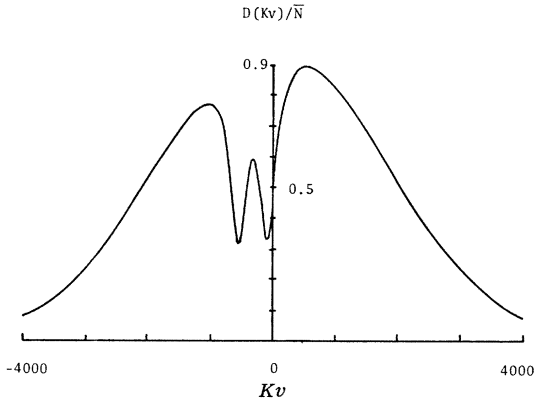

FIG. 10. Graph of normalized population difference vs Kv for a rotating bidirectional ring laser. The figure is for exaggerated parameters, as may result from a multiturn ring laser rate gyro. $\Delta_r = 6\gamma$, average detuning $= 2\gamma$, $\gamma_a = \gamma_b = \gamma = 100$ MHz, $Ku = 25\gamma$, relative excitation $= 2.0$. Note that the holes are symmetrically spaced by 2γ from zero average detuned position of $-\frac{1}{2}\Delta_r = -3\gamma$.

tioned with respect to the Gaussian velocity distribution, and cause a corresponding amplitude asymmetry in the population difference (see Fig. 10). Such asymmetry contrasts with the nonrotating case and with the two-mirror, standing-wave lasers, which have holes symmetrically located about the center of the velocity distribution.

It is helpful to note that a simple change of variables shifts the origin by an amount equal to the rotational shift, symmetrically locating the holes and displacing the Gaussian velocity distribution. The integral for the polarization (18) is then given by

$$\mathcal{P}_n = -\frac{i\epsilon_0 \mathfrak{N}}{Q\sqrt{\pi}\, Z_i(\gamma)} \sum_{m=1}^{2} E_m e^{i(\phi_n - \phi_m)} \int_{-\infty}^{\infty} d\omega' \exp\left(\frac{-(\omega' - \frac{1}{2}\Delta_r - \omega_0)^2}{\Delta\omega^2}\right) \mathfrak{D}(\omega' - \nu_n) d_{m-n}(\omega'),$$

where $\omega' = \omega + \frac{1}{2}\Delta_r$. It is interesting to observe that the sum of the two equations for $\mathcal{P}_1$ and $\mathcal{P}_2$ is identical with the equation for the ordinary two-mirror, standing-wave laser except that the Gaussian is shifted (we also have a factor of 4 appearing in the interpretation of the intensities). For this equal-mode-intensity case and symmetric tuning, we can write the population-difference and polarization Fourier coefficients d_k and p_m in terms of Bessel functions as has been done for the two-mirror, standing-wave laser.[13]

Unequal mode intensities break the symmetry. The amount of asymmetry is determined by the fractional intensity splitting and arises from the $C_{0,k}$ (and S_k) terms in Eq. (I 67). The $C_{0,k}$ term may be written

$$C_{0,k} = [\mathfrak{F}(k\Delta)]^{-1} + \tfrac{1}{2}(I_1 + I_2)[\mathfrak{D}(\nu_{1+k} - \omega) + \mathfrak{D}(\omega - \nu_{2-k}) + \mathfrak{D}(\nu_{2+k} - \omega) + \mathfrak{D}(\omega - \nu_{1-k})]$$
$$+ \tfrac{1}{2}[(I_1 - I_2)/I_{av}]I_{av}[\mathfrak{D}(\nu_{1+k} - \omega) - \mathfrak{D}(\omega - \nu_{2-k}) - \mathfrak{D}(\nu_{2+k} - \omega) + \mathfrak{D}(\omega - \nu_{1-k})],$$

where symmetric displacement about the rotationally shifted position interchanges the roles of the terms in a pairwise fashion, yielding the complex conjugate for equal intensities. However, the terms proportional to the fractional intensity splitting behave differently, producing asymmetry about the rotationally shifted position. Another important symmetry property follows from the fact that for a given value of average detuning the hole burning term S_k remains the same if we change the sign of the average detuning and simultaneously interchange the roles of the two intensities I_1 and I_2. Similar observations may be made for the remaining terms contributing to the population-difference coefficients d_k. Consequently, we would expect that a curve of mode intensities versus cavity detuning should be symmetrical about the origin if we interchange the roles of the intensities when passing through the origin. This result is highly useful since we need only compute and plot one-half of the curve. Symmetry properties predict equal mode intensities at zero average detuning. This result is somewhat modified when we have regions of hysteresis about the origin as in bistable operation, in which case we must remain on the same leg of the hysteresis loop when interchanging intensities while passing through the origin. In this case a stable solution may not exist for equal mode intensities at zero average detuning.

Recalling discussion in Sec. III of fractional intensity splitting for the general two-mode case, let us examine in this framework the role played by the asymmetry induced by the rotational shift. Again looking at the population-difference hole-burning term S_k, we see that for zero average detuning we have one hole burned in the population difference at the rotationally shifted position. In the near Doppler limit for this case we have equal linear net gains and nearly equal self- and cross-saturation terms. For the asymmetrically tuned case, because of the rotationally induced asymmetry of the holes, we have unequal linear net gains for the two modes; thus we should expect some fractional intensity splitting. For small-average-detuned operation, the mode having higher intensity would be predicted to be the one with higher linear net gain. This would be expected to be the case for the hole nearest the origin. Interchanging the holes, such as would occur if the sense of rotation were reversed, would cause the roles of the intensities to be interchanged. Thus for bistable operation, if for a given sense of rotation and scan direction mode 1 dominated, then with a change in the direction of rotation mode 2 should dominate rather than mode 1. This dependence of the dominant-mode selection on the sense of rotation has been observed experimentally.[4]

The magnitude of the fractional intensity splitting is determined both by the fractional gain difference and by the magnitude of the coupling parameter C. In this respect let us consider the region of relative excitation values from 1 to 1.2, which historically has been considered to be the domain of the third-order theory. In this region of low

intensities we would expect the fractional gain differences to be rather large and lead to large fractional intensity splitting phenomena. However, the effect of population pulsations enter into the coupling parameter C and profoundly affect the problem. As the theories being compared (REA, third order, and strong signal) differ in the presence and importance of population pulsations, the theories vary in their predicted fractional intensity splittings. The coupling parameter C is given in the Doppler-limit third-order theory by a simple Lorentzian (of average detuning) squared [Ref. 10, Eq. (11-17)]. It becomes increasingly important as its value approaches unity, namely, for symmetric tuning. Thus in the wings of the tuning curve we expect moderate fractional intensity splitting, while near symmetric tuning we expect it to increase dramatically.

In the Doppler-limit third-order case, complete mode inhibition is predicted. Figure 9 illustrates this for a relative excitation value of 1.05, which is well within the historical third-order domain. Figure 8 illustrates the near Doppler limit which predicts true self-induced bistable operation with a resulting single-traveling-wave (STW) region near symmetric tuning, caused by an overestimation of the Bragg scattering. This is in agreement with the results predicted earlier in Ref. 6 and would tend to agree with experimental results of Moss *et al.*[14] However, for the particular laser parameters chosen, the stability coupling parameter C^{Sm} is very near unity ($C^{Sm}=0.995$) at symmetric tuning. This implies only a slight tendency for strong coupling. For very low values of relative excitation (1.01), the strong-signal results also predict true self-induced bistable operation in agreement with the third-order results. This is to be expected, since the third-order theory is an expansion about threshold values of intensity $0+\epsilon$ and here ϵ is quite small. Thus in this region of extremely low intensities, we have made firm connection with the third-order theory. This region will be referred to as the true third-order domain.

We find that such exact agreement does not extend throughout the entire region of relative excitation of 1.0 to 1.2. We refer to the region of nonagreement as the pseudo-third-order domain. The lower limit of the pseudo-third-order domain may vary widely with such factors as laser detuning and is especially sensitive to the laser parameters (level decay, etc.). Such sensitivity is in agreement with the third-order results predicted earlier[6]; however, the intensity dependence of the coupling parameter was not included. The strong-signal results predict that the stability coupling parameter C^{Sm} is a decreasing function of intensity (hence relative excitation) in the third-order domain. Consequently, for a given set of laser parameters at some point, as the relative excitation is increased, C^{Sm} becomes less than unity and true self-induced bistable operation is replaced by stable bidirectional operation with equal mode intensities at symmetric tuning. The sensitivity to the laser parameters is illustrated by the fact that for a relative excitation value of 1.05 the dividing line between these two regions is given by $Ku=6.5\gamma$. At $Ku=10.10\gamma$, a value also commonly used for He-Ne laser operation, the solutions are not bistable. It is to this pseudo-third-order region that we now turn.

In the psuedo-third-order domain the strong-signal coupling parameter is less than that of the third-order theory. Consequently, the ratio $1/(1-C)$ entering into the fractional intensity splitting may be substantially smaller near symmetric tuning for the strong-signal theory than for the third-order theory. Thus the extremely large fractional intensity splitting predicted by the third-order theory is not in general predicted by the strong-signal theory. It must be recalled that the splitting is dependent upon the relative excitation. For a low relative excitation value of 1.05 (see Fig. 6), appreciable fractional intensity splitting is predicted by the strong-signal theory, while at a higher value of 1.2 a considerably smaller amount is predicted. This contrasts with the complete mode inhibition predicted by the Doppler-limit third-order theory and bistable STW operation predicted by the generally broadened third-order theory. In addition, the third-order theory does not correctly predict the average intensity in a manner similar to that encountered in prior work done on the two-mirror, standing-wave laser.[12]

Reference 12 also shows that for these low intensities, the standing-wave, REA, and strong-signal theories agree quite well as to the predicted intensities. At first glance this would seem to indicate that the fractional intensity splitting predicted by both would be approximately the same. This is the case for detuned operation as in the wings of the tuning curve, but not near symmetric tuning where population pulsations become increasingly more important. In this region the REA coupling parameter is larger than that of the strong-signal theory and in fact has a value equal to or nearly equal to unity in a small region on either side of symmetric tuning. This causes large fractional intensity splitting near these regions and complete mode inhibition within them. Figure 7 illustrates this. While most pronounced at these low values, this mode inhibition is present at higher values of relative excitation.

As previously mentioned, in the pseudo-third-

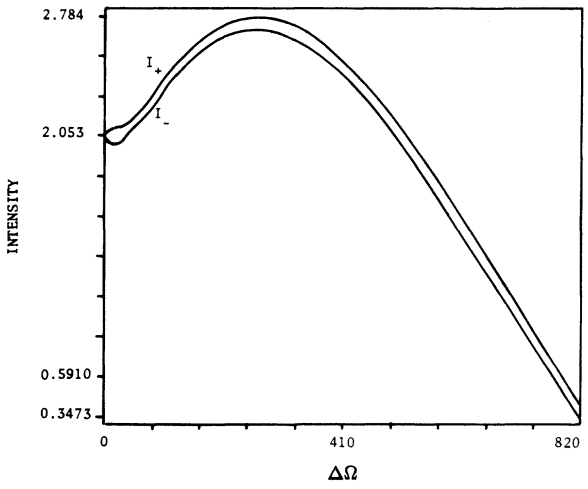

FIG. 11. Graph of the strong-signal theory bidirectional ring laser intensities vs average cavity detuning for a relative excitation of 2.0. Note the small fractional intensity splitting near the origin and the overall similarity to a Lamb dip. Laser parameters are the same as in Fig. 6.

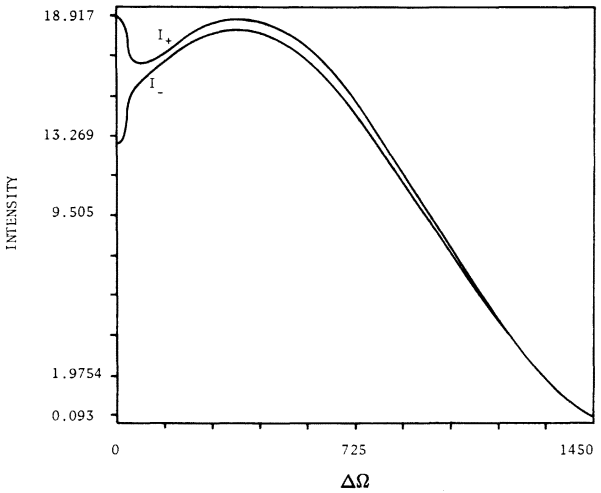

FIG. 13. Graph of the strong-signal theory bidirectional ring laser intensities vs average cavity detuning for a relative excitation of 6.0. Only one leg of the hysteresis path is shown. The laser parameters are the same as in Fig. 6.

order region the fractional intensity splitting was a decreasing function of relative excitation. This behavior continues until the two modes give the appearance of being completely uncoupled even though the cross-saturation terms (θ^{Sm}) are not zero and may be nearly equal to the self-saturation terms (β^{Sm}). Figures 11 and 12 illustrate this effect at a relative excitation value of 2.0. It might be noted that the REA theory still gives complete mode inhibition about the origin.

At high values of intensities (and corresponding

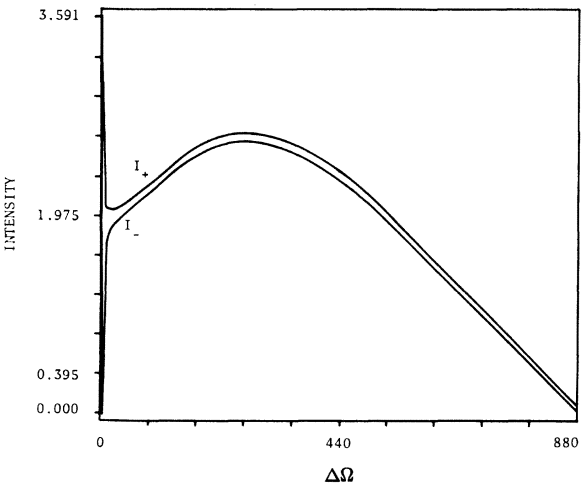

FIG. 12. Graph of the REA theory bidirectional ring laser intensities vs average cavity detuning for a relative excitation of 2.0. Note the mode inhibition near the origin. The laser parameters are the same as in Fig. 6.

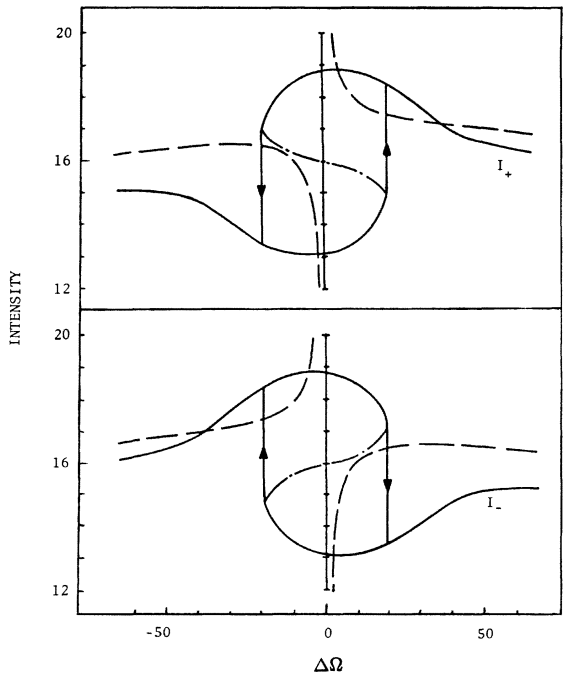

FIG. 14. Graph of the bistable region of bidirectional ring laser operation at a relative excitation of 6. The curves are intensity vs average cavity detuning. The dashed line corresponds to the REA solution. The dashed-dot line is the unstable strong-signal curve. The solid line is the hysteresis path for the strong-signal stable solution. The arrows originate from a point of neutral coupling and indicate a jump to the other leg of the path when passing through that point. The laser parameters are the same as in Fig. 6.

high relative excitations), because of the extreme nonlinearity of the problem, multiple-valued solutions may be obtained. The several solutions may connect through regions of neutral coupling and give rise to hysteresis paths in the intensity-vs-detuning curves. This yields bistable operation where both modes may have nonzero intensities as opposed to the single-traveling-wave form of bistable operation noted for lower intensities. Figures 13 and 14 illustrate this for a value of relative excitation of 6.0. It is interesting to note that an unstable solution exists which passes through the tuning origin with equal mode intensities. The REA solution is single valued and still exhibits mode inhibition about the origin with equal intensities at the origin. Again citing work done on the two-mirror, standing-wave laser, the average intensity predicted near symmetrical tuning for the REA is also less than the strong-signal results for the bidirectional ring.[12]

The two-mode unidirectional ring laser has two holes burned in the population-vs-velocity curve, one for each mode. Since they do not share a common set of atoms, there is relatively little interaction between the modes (if $\Delta > \gamma$). The curves of intensity versus detuning for the strong-signal case are similar to the third-order results of Ref. 11. For the strong-signal case, the two modes oscillated above threshold over a larger range of detuning than in the REA case. In addition, at symmetric tuning the strong-signal intensity was about 2% greater than the REA intensity. This point deviated slightly from the otherwise smooth curve. The REA had a slight bump while the strong-signal theory gave a slight dip (less than 1% in both cases).

The relatively weak interactions in the unidirectional case allowed the integration step size to be $\frac{1}{2}\gamma$ or $\frac{1}{4}\gamma$ in the evaluation of the polarization integral (18). This contrasts with the small step size of $\frac{1}{16}\gamma$ or $\frac{1}{32}\gamma$ required for the bidirectional ring.

VI. UNIDIRECTIONAL MULTIMODE LOCKED OPERATION

In unidirectional multimode operation the signals mix in the nonlinear medium and produce population pulsations at integral multiples of the mode spacing Δ. These pulsations interact with the original signals to produce sideband signals spaced multiples of Δ from the original frequencies. We have already discussed the effect of some of these sidebands on the cross saturation in two-mode operation. For three- and higher-mode operation the remaining sidebands produce a different kind of coupling in acting like injected signals. For example, in three-mode operation, ν_2 beats with $\Delta = \nu_2 - \nu_1$, producing a term at ν_3, say, ν_3'. This sideband interacts with the ν_3 signal influencing its phase, amplitude, and frequency very much like the injected signal in Van der Pol's triode oscillator.[15] There the oscillator "locked" onto the injected signal when the frequency difference was sufficiently small. The sideband near $\nu_1(\nu_1')$ behaves similarly owing to ν_2 and ν_3. The result can be frequency locking, i.e., equal beat notes between adjacent modes.

Salomaa and Salomaa[7] treated three-mode mode-locked operation in the third-order theory, but were not able to obtain mode-locked solutions in the Fourier theory. Our strong-signal results for their laser parameters exhibit mode locking and are presented in Fig. 15. The relative phase ranges from about $-60°$ to $+60°$. The numerical procedure for zeroing the self-consistency equations (I 5) and (I 6) failed to converge for large detuning. This may be due to one of three possible problems: (i) the method is incapable of treating the configuration, (ii) no solution exists, or (iii) more than one solution exists, the stability of which is uncertain. The numerical procedure "behaved" as if two solutions existed.

Salomaa and Salomaa[7] found oscillating solutions for this range in their strong-signal treatment. The intensities we obtained are equal to within 5–10% (graph interpretation error) of the temporal

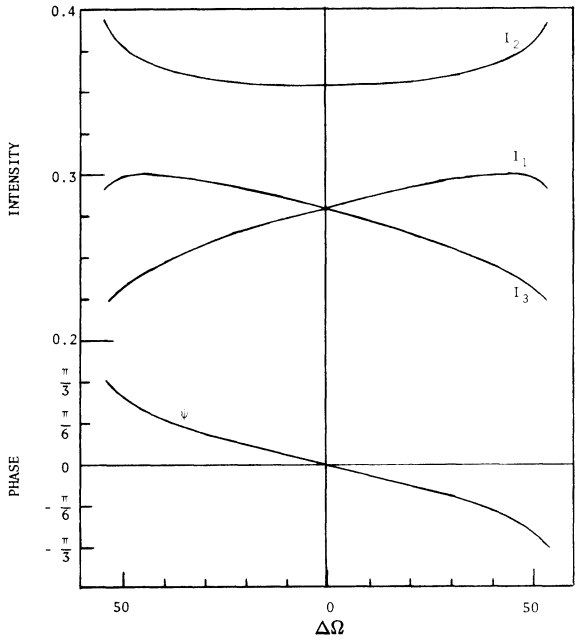

FIG. 15. Graph of the relative phase and intensities vs cavity detuning for the three-mode unidirectional ring laser at a relative excitation of 1.5. The detuning indicated is that of the central mode (2). The mode spacing = 400 MHz, $\gamma_a = \gamma_b = \gamma = 100$ MHz, and $Ku = 1000$ MHz.

average of these solutions (cf. their Fig. 21). For zero average detuning ($\nu_1+\nu_2+\nu_3=3\omega$), the eigenvalues of the stability matrix F of Eq. (I 99) are negative and real. As this detuning is increased, the eigenvalues acquire imaginary parts of increasing magnitude. The presence of these nonzero imaginary parts leads to oscillations in the mode intensities and phases as they approach steady state in time. This may well explain Salomaa and Salomaa's oscillations and indicate they did not integrate the self-consistency equations long enough to find the steady-state solutions. Their third-order mode-locked results exhibited a dip or "hole" in all three intensities in the center of the mode-locked region. This dip as defined by I_2 was about 50 MHz wide. We find mode-locked strong-signal operation over a wider region (100 MHz), which is comparable to their Fourier non-mode-locked results for the central mode I_2; however, they did not find such a dip in the two side intensities. Our mode-locked results tend to exhibit a slight dip as shown by the extremities of the curves of I_1 (54 MHz) and I_3(−54 MHz). This tends to support the connection of a dip with mode locking.

In addition to comparison with the Salomaa and Salomaa results, we explored solutions with laser parameters which contained level decays more

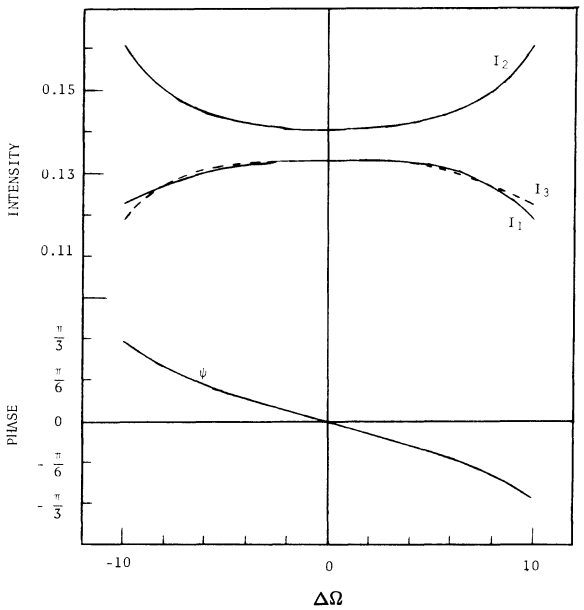

FIG. 16. Graph of the relative phase and intensities vs cavity detuning for the three-mode unidirectional ring laser at a relative excitation of 1.1. The detuning indicated is that of the central mode (2). The mode spacing = 150 MHz, γ_a = 20 MHz, γ_b = 40 MHz, γ = 100 MHz, Ku = 1010 MHz.

representative of He-Ne operation. We chose $\gamma_a=20$, $\gamma_b=40$, and $\gamma=100$ MHz, with the mode separation equal to 150 MHz. The results obtained for a value of relative excitation of 1.1 are presented in Fig. 16. The mode-locked region explored was smaller in width (20 MHz) for the same range of relative phase as in the Salomaa and Salomaa data.

The rate-equation results for symmetric tuning are $I_1=I_3=0.0892$, $I_2=0.1947$, compared to $I_1=I_3=0.1333$, $I_2=0.1404$ for the strong-signal case. The central mode is larger than that of the strong-signal results, whereas the side modes are lower. For higher relative excitation and symmetric operation, the side modes may be larger than the central mode in the strong signal theory. Salomaa and Salomaa noted this only for detuned operation. For a relative excitation of 2.0, complete suppression of the central mode may occur. These mode interactions may be interpreted as due to two effects: (i) The central mode competes directly for atoms with the two side modes owing to standard two-mode cross saturation. In the strong-signal theory population pulsations contribute to this cross saturation through the population-depletion term S_p in (14). (ii) Pump power can be transferred from the atomic velocity ensemble nearly resonant with the center mode to those of the side modes by mixing processes associated with "injected signals" or combination tones. This is analogous to the mixing in a passive radio frequency device such as a silicon diode. With two input signals (ν_1 and ν_2) of constant power, the mixer output consists of combination tones and harmonics. One of these sidebands has frequency ν_3 derived in part through the relationships

$$\nu_3=\nu_2+(\nu_2-\nu_1) \quad \text{and} \quad \nu_3=\nu_1+2(\nu_2-\nu_1).$$

This signal at ν_3 derives its power from the two input signals at ν_1 and ν_2; hence we have a transfer of power from ν_1 and ν_2 to ν_3. In the laser the "input" signals ν_1 and ν_2 derive their power from the pump power via those atoms which are nearly resonant with the signals, i.e., $Kv=\nu_1\pm\gamma$, $\nu_2\pm\gamma$. This pump power may be transferred from ν_1 and ν_2 to ν_3. Such transference may be appreciable (10%). If the target mode ν_3 is already oscillating, the transference may help or hinder that mode. An oscillating ν_3 can, in turn, transfer power from itself and ν_2 back to ν_1. Thus, the side modes may gain power at the expense of ν_2 (for $\Delta<\gamma,\gamma_a,\gamma_b$, the opposite may be true). In particular we find from third-order theory that the power is transferred from ν_2 to ν_1 and ν_3 provided

$$\frac{1}{\gamma_a}\mathfrak{L}_a(\Delta)\left(1-\frac{\Delta^2}{\gamma\gamma_a}\right)+\frac{1}{\gamma_b}\mathfrak{L}_b(\Delta)\left(1-\frac{\Delta^2}{\gamma\gamma_b}\right)<0.$$

This follows from evaluation of the ϑ_{1232}, $\vartheta_{2123} + \vartheta_{2321}$, and ϑ_{3212} expressions of Ref. 11 for unidirectional operation. In the strong-signal theory, an example of this transference would be the contribution to the polarization (18) from d_1 and d_2. We may make a modified rate-equation approximation in which we suppress the final-step sidebands generated by the modulator, i.e., keep only the dc population-difference term d_0 in Eq. (18). Sidebands occurring in higher-order beating processes that contribute to d_0 are kept via S_p in contrast to the ordinary REA. This gives a feel for the dc saturation effect (through d_0) compared to the final-step power transfer processes. The results of this approximation are $I_1 = I_3 = 0.090$, $I_2 = 0.190$, which are close to the REA results in this case. Hence the substantial difference between the REA and strong-signal predictions is primarily due to the final-step power transfer processes.

A possible explanation of the null locking results of Salomaa and Salomaa may be found in the numerical method used for their solutions. While we solved for steady-state solutions directly, they chose to solve the self-consistency equations (5) and (6) of I by a Runge-Kutte–type Merson algorithm. They started with small values of intensities (0.001) and zero for the relative phase, and allowed the integration to proceed until stable steady-state solutions were found (which did not occur). The accuracy in the transient region was 5% for the Fourier theory as compared to 10^{-3}% for the third-order case which was successful. This inaccuracy combined with a large step size of γ for the evaluation of the polarization integrals probably caused enough error in the procedure such that the oscillating transient solutions never decayed. Another possible source of error could be limited computational accuracy. For the mode-locking conditions to be accurately satisfied 10–12 digits are needed. In this respect our REA solutions for the Salomaa and Salomaa data gave "mode-locked" errors of 1000 Hz at a detuning of 50 MHz. This may be taken as an indication of the minimum error to assume for mode-locking. We chose 1 Hz and typically obtained 0.1 Hz or better.

ACKNOWLEDGMENT

It is a pleasure to acknowledge helpful conversations with Professor W. E. Lamb, Jr.

APPENDIX: BIDIRECTIONAL GAIN COEFFICIENT

In this appendix we derive Eq. (39) for the strong-signal gain of a homogeneously broadened medium subject to a two-mode bidirectional ring laser field. We suppose that the mode frequencies and wave numbers are equal ($\nu_+ = \nu_- = \nu$, $K_+ = K_- = K$), but allow the intensities to vary. This is obviously a special case, but it does provide some insight into the nature of the saturation mechanics. In the REA the equations of motion (I 28) and (I 29) for the populations have the steady-state solution

$$D(z) = \rho_{aa} - \rho_{bb} = N(z)/[1 + S_h + S_p \cos(2Kz)] \ , \quad \text{(A1)}$$

where the hole-burning term is

$$S_h = 2(\gamma_{ab}/\gamma)\mathfrak{L}(\omega - \nu)(I_+ - I_-) \quad \text{(A2)}$$

and the population-pulsation term (note that here there are no pulsations since $\nu_+ = \nu_-$) is

$$S_p = 4(\gamma_{ab}/\gamma)\mathfrak{L}(\omega - \nu)(I_+ I_-)^{1/2} . \quad \text{(A3)}$$

The polarization matrix element ρ_{ab} of Eq. (I 27) is given by

$$\rho_{ab} = -\tfrac{1}{2}(\wp/\hbar)\mathfrak{D}(\omega - \nu)D(z)(E_+ e^{iKz} + E_- e^{-iKz}),$$

yielding the polarization component of Eq. (19) as

$$\mathcal{P}_\pm = -i\,\frac{\wp^2}{\hbar}\mathfrak{D}(\omega - \nu)\,\frac{1}{L}\int_0^L dz\,\frac{\exp(\mp iKz)N(z)}{1 + S_h + S_p\cos(2Kz)} \times (E_+ e^{iKz} + E_- e^{-iKz})$$

$$= -i(\wp^2/\hbar)\mathfrak{D}(\omega - \nu)\bar{N}J_\pm . \quad \text{(A4)}$$

Here the integrals $J_\pm$ are given by

$$J_\pm = \frac{1}{2\pi}\int_0^{2\pi} dx \frac{E_\pm + E_\mp \exp(\mp ix)}{1 + S_h + S_p\cos(x)}$$

$$= \frac{1}{2\pi}\int_0^{2\pi} dx\,\frac{E_\pm + E_\mp\cos(x)}{1 + S_h + S_p\cos(x)} . \quad \text{(A5)}$$

These may be evaluated by straightforward means and are seen to be

$$J_\pm = E_\pm[(1 + S_h)^2 - S_p^2]^{-1/2} + \frac{E_\mp}{S_p}\left(1 - \frac{1 + S_h}{[(1 + S_h)^2 - S_p^2]^{1/2}}\right)$$

$$= \frac{E_\mp}{S_p}\left(1 - \frac{1 + S_h - E_\pm S_p/E_\mp}{[1 + 2S_h + 4\mathfrak{L}^2(I_+ - I_-)^2]^{1/2}}\right) . \quad \text{(A6)}$$

This with Eq. (A4) for $\mathcal{P}_\pm$ and Eq. (I 86) yields Eq. (39) of the text.

---

*This paper is based in part on material submitted by J. B. Hambenne in partial fulfillment of the requirements for the degree of Doctor of Philosophy at the University of Arizona. Supported in part by the Air Force Weapons Laboratory (Kirtland) and in part by the Space and Missile Systems Organizations (Los Angeles).

†Address June 1975–76: Max Planck Institut and Universität Stuttgart, Stuttgart, Germany.

[1] J. B. Hambenne and M. Sargent III, preceding paper,

Phys. Rev. A 13, 784 (1976).
[2]G. Sagnac, C. R. Acad. Sci. (Paris) 157, 708 (1913).
[3]W. M. Macek and D. T. M. Davis, Jr., Appl. Phys. Lett. 2, 67 (1963).
[4]F. Aronowitz, Appl. Opt. 11, 405 (1972).
[5]F. Aronowitz and R. J. Collins, Appl. Phys. Lett. 9, 55 (1966).
[6]J. B. Hambenne and M. Sargent III, IEEE J. Quan. Elect. QE-11, 90 (1975). See also K. Takata [Jpn. J. Appl. Phys. 11, 699 (1972)], who did not use a Bragg-scattering interpretation.
[7]M. Salomaa and R. Salomaa, Phys. Fenn. 8, 289 (1973).
[8]A equation number (I 10) refers to Eq. (10) of paper I, etc.
[9]L. N. Menegozzi and W. E. Lamb, Jr., Phys. Rev. A 8, 2103 (1973).
[10]M. Sargent III, M. O. Scully, and W. E. Lamb, Jr., *Laser Physics* (Addison-Wesley, Reading, Mass., 1974).
[11]C. L. O'Bryan III and M. Sargent III, Phys. Rev. A 8, 3071 (1973).
[12]S. Stenholm and W. E. Lamb, Jr., Phys. Rev. 181, 618 (1969).
[13]B. J. Feldman and M. S. Feld, Phys. Rev. A 1, 1375 (1970).
[14]T. S. Moss, D. E. Killick, and E. T. de la Perrelle, Infrared Phys. 4, 209 (1964).
[15]B. van der Pol, Inst. Radio Eng. 22, 1051 (1934).